# A BULK-FLOW ANALYSIS OF A NOVEL GAS DAMPER SEAL

by

Jiming Li
Dr. Luis San Andrés
Dr. John Vance

May 1997

TL-SEAL-2-97

Support for this research effort is provided by the *Advanced Technology Program, State of Texas.* Project *32190/71700/ME*, October 1995-October 1997.

TABLE OF CONTENTS


LIST OF TABLES . . . . . 2
LIST OF FIGURES . . . . . 3
NOMENCLATURE . . . . . 4
EXECUTIVE SUMMARY . . . . . 6
INTRODUCTION . . . . . 6
A BULK-FLOW MODEL OF GAS DAMPER SEALS . . . . . 10
Governing equations . . . . . 10
Shear stress model . . . . . 11
Boundary conditions . . . . . 12
Zeroth-order and first-order perturbationequations . . . . . 13
Numerical method of solution . . . . . 16
Seal dynamic forces and force coefficients . . . . . 17
VALIDATION OF THE BULK-FLOW MODEL . . . . . 18
Comparison to existing test results for a two-bladed gas damper seal . . . . . 18
A numerical example of a two-bladed gas labyrinth seal . . . . . 20
Comparisons to limited test data for a two-bladed see-through gas labyrinth seal 22
DYNAMIC PERFORMANCE OF A TWO-BLADED GAS DAMPER SEAL . . . . . 23
The effect of the rotor speed on the dynamic force coefficients . . . . . 23
The effect of the pre-swirl velocity on the dynamic force coefficients . . . . . 24
The effect of the supply pressure on the dynamic force coefficients . . . . . 24
The effect of the excitation frequency on the dynamic forces . . . . . 25
The effect of the modulated vs.fixed exit clearance on the dynamic performance 25
CONCLUSIONS . . . . . 26
ACKNOWLEDGEMENTS . . . . . 27

LIST OF TABLES

Table Page

1. Two-bladed gas damper seal dimensions and operating conditions for rap tests (Li, 1995) . . . . . 19
2. A see-through two-teeth gas labyrinth seal dimensions and operating conditions for theoretical predictions . . . . . 21
3. A see-through two-teeth gas labyrinth seal dimensions and operating conditions (Wright, 1983) . . . . . 22

LIST OF FIGURES


Figure Page

1. Schematic of a two-bladed gas damper seal with four partition walls . . . . . 28
2. One control volume model for gas damper seals . . . . . 29
3. Experimental values and computed predictions of mass flow rates for a two-bladed gas damper seal vs. inlet pressure . . . . . 30
4. Experimental values and computed predictions for direct damping coefficients of a two-bladed gas damper seal ($\Omega$=0.0 rpm, $\omega$=66 Hz) . . . . . 30
5. Computed predictions for direct stiffness coefficients of a two-bladed gas damper seal( $\Omega$ = 0.0 rpm, $\omega$ = 66 Hz ) . . . . . 31
6. Static characteristics of a two-teeth labyrinth seal vs. inlet pressure . . . . . 32
7. Damping coefficients of a two-teeth labyrinth seal vs. inlet pressure . . . . . 33
8. Stiffness coefficients of a two-teeth labyrinth seal vs. inlet pressure . . . . . 33
9. Experimental and theoretical Mass flow rates for a see-through labyrinth seal at two back pressures (Wright, 1983) . . . . . 34
10. Experimental and theoretical tangential dynamic forces for a see-through labyrinth seal at two back pressures (Wright, 1983) . . . . . 34
11. Experimental and theoretical radial dynamic forces for a see-through labyrinth seal at two back pressures (Wright, 1983) . . . . . 35
12. Dynamic force coefficients of a two-bladed gas damper seal vs. rotor speed . . . 36
13. Dynamic force coefficients of a two-bladed gas damper seal vs. inlet pre-swirl ratio . . . . . 37
14. Dynamic force coefficients of a two-bladed gas damper seal vs. inlet pressure . . 38
15. Dynamic forces of a two-bladed gas damper seal vs. excitation frequency for two pre-swirl ratios . . . . . 39
16. Dynamic forces of a two-bladed gas damper seal vs. excitation frequency at two inlet pressures . . . . . 39
17. Dynamic force coefficients of a two-bladed gas damper seal with fixed and modulated exit clearances . . . . . 40
18. Radial and tangential dynamic forces of a two-bladed gas damper seal with fixed and modulated exit clearances . . . . . 41

## NOMENCLATURE

| | |
|---|---|
| $A$ | $L(B+H)$, cross-section area of the cavity [m$^2$] |
| $B$ | height of the seal teeth [m] |
| $C_{ij}$ | damping coefficients [N-s/m], $i, j = X, Y$ |
| $D_h$ | $2L(B+H)/(L+B+H)$, hydraulic diameter of the seal [m] |
| $e$ | $(e^2_X + e^2_Y)^{1/2}$, rotor orbit amplitude [m] |
| $e_X$, $e_Y$ | rotor displacements in the X and Y directions |
| $e_r$, $e_s$ | mean roughness at rotor and stator surfaces |
| $F_j$ | dynamic seal forces [N], $j = X, Y$ |
| $F_r$ | $-(K_{XX} + \omega C_{XY})e$, radial dynamic seal forces [N/m] |
| $F_t$ | $-(\omega C_{XX} - K_{XY})e$, tangential dynamic seal forces [N/m] |
| $H$ | seal clearance [m] |
| $K_{ij}$ | stiffness coefficients [N/m], $i, j = X, Y$ |
| $L$ | inside length of the cavity [m] |
| $\dot{M}$ | mass flow rate resulting from pressure drop [kg/m-s] |
| $N_c$ | number of circumferential pockets |
| $P$ | fluid pressure in seal cavity [N/m$^2$] |
| $P_b$ | back pressure at seal exit [N/m$^2$] |
| $P_s$ | supply pressure at seal entrance [N/m$^2$] |
| $R_a$ | $(R_r+R_s)/2$, average seal radius [m] |
| $R_g$ | gas constant [J/kg-°K] |
| $R_r$ | rotor radius [m] |
| $R_s$ | seal outside radius [m] |
| $Re_r$ | $\rho D_h[(U-\Omega R_r)^2+W^2]^{1/2}/\mu$, local Reynolds number at the rotor surface |
| $Re_s$ | $\rho D_h(U^2+W^2)^{1/2}/\mu$, local Reynolds number at the stator surface |
| $T$ | gas temperature [°K] |
| $U$ | circumferential bulk-flow velocity in seal cavity [m/s] |
| $U_s$ | pre-swirl velocity of gas flow at seal entrance [m/s] |
| $V_*$ | $(R_gT)^{1/2}$, characteristic speed of gas [m/s] |
| $W$ | axial bulk-flow velocity [m/s] |
| $\alpha_{in}$ | inlet pre-swirl velocity ratio |
| $f_r$, $f_s$ | $a_m\{1 + [c_m e_{r,s}/(B+H) + b_m/Re_{r,s}]^{e_m}\}$ Moody's friction factors at the rotor and stator surfaces $a_m=0.001375$; $b_m=10^6$; $c_m=10^4$; $e_m=1/3$ |
| $\mu_c$ | "kinetic-energy carryover" factor of gas flow across seal teeth |

| | |
|---|---|
| $\mu_f$ | gas flow coefficient across seal teeth |
| $\tau_r$ | shear stress acting on the rotor surface |
| $\tau_s$ | shear stress acting on the stator surface |
| $\varsigma_r$ | $R_r / R_a = 2 / (1 + R_s / R_r)$ |
| $\varsigma_s$ | $R_s / R_a = 2 / (1 + R_r / R_s)$ |
| $\rho$ | gas density [kg/m$^3$] |
| $\mu$ | gas viscosity [N-s/m$^2$] |
| $\gamma$ | ratio of specific heats, 1.4 for gas typically |
| $\Omega$ | angular speed of rotor [rad/s] |
| $\omega$ | angular whirling frequency of the rotor [rad/s] |

Subscripts:

| | |
|---|---|
| $0$ | refers to zeroth-order solution |
| $i, j$ | refer to first-order solutions ( $i, j = X, Y$ ) |
| $s$ | refers to seal upstream |
| $b$ | refers to seal downstream |
| $u$ | refers to local upstream |
| $d$ | refers to local downstream |
| $w$ | refers to partition wall |

## EXECUTIVE SUMMARY

A bulk-flow model for determination of the dynamic force characteristics of a novel gas damper seal with partition walls dividing the seal circumferential groove into several cavities is presented. The model can also be applied to conventional gas labyrinth seals. Perturbation equations for the seal cavity flow, flow across the partition walls, and axial mass flow rate are derived for a centered seal condition. Flow turbulence is accounted for by using turbulent shear stress parameters and Moody's friction factors in the circumferential bulk-flow momentum equation. The flow equations are numerically solved and a computer program is developed correspondingly. Theoretical predictions from the current model are compared to limited experimental results and computed results for a two-bladed gas damper seal and a two two-bladed gas labyrinth seal. Numerous computational results illustrate the effects of inlet pressure, rotor speed and whirl frequency on the rotordynamic force characteristics of a two-bladed gas damper seal with four partition walls. Moreover, the dynamic performance of a gas damper seal with fixed and modulated exit clearances is also evaluated.

## INTRODUCTION

Von Pragenau (1982) first describes damper-seals for use in turbopumps, by reducing the mean swirl velocity in annular pressure seals with a roughened stator, and thereby reducing or eliminating destabilizing hydrodynamic forces. One of the advantages of damper seals, as compared to fluid film journal bearings or squeeze film dampers, is that they can be installed along the rotor at locations which have large modal amplitudes. Hence, damper seals have the potential of more effectively suppressing rotor vibrations.

A number of experimental investigations have been carried out to achieve rotordynamically stable gas seal configurations since the mid 1980's. Brown and Hart (1986) introduce an anti-swirl gas damper which has a number of tangential nozzles discharging in the opposite direction to the rotor motion. Experimental results show the synchronous response of the rotor to be considerably reduced at critical speeds and with the corresponding critical speeds rising. It is simple to realize an active control of rotor vibration since the anti-swirl damper may

be activated only when required. Kim and Lee (1994) test three annular liquid seals with an anti-swirl self-injection mechanism. Experimental results show that the whirl frequency ratio is significantly reduced as compared to a damper seal with a hole-pattern stator surface, however the leakage performance of the anti-swirl seals is degraded. On the other hand, Vance and Handy (1996) demonstrate that a backward instability could be promoted by an improperly designed anti-swirl gas damper.

Annular gas damper seals with various types of machined *rough* surfaces have been investigated. Childs, et. al.(1989, 1990a and 1993) experimentally verify that a long honeycomb gas seal is more effective to reduce the cross-coupled stiffness and provide more direct damping than a short honeycomb gas seal. Typically, honeycomb seals are more stable than annular smooth seals and labyrinth seals. Honeycomb seals have been successfully used in industrial compressors to replace labyrinth seals for suppressing subsynchronous vibrations (Zeidan et al., 1993). As a design alternative to the honeycomb seal, a type of hole-pattern gas damper seals has been tested by Yu and Childs (1997). The experiments show that the hole-pattern gas damper seal provides higher effective damping and lower leakage rate than a conventional honeycomb seal.

Childs, et al. (1990b) first mention that the rotordynamic force coefficients for some types of gas seals are frequency dependent. Recently, Kleynhans and Childs (1996) develop a simplified acoustic model to illustrate that the conventional assumption of frequency-independent force coefficients is invalid for honeycomb seals. In brief, the honeycomb cell volume causes a dramatic reduction in the flow lowest acoustic frequency and affects the seal dynamic forced response.

Childs and Gansle (1996) study the rotordynamic force characteristics of grooved annular gas seals with different helix angles directed against rotation. The tests results show that the cross-coupled stiffness steadily decreases as the helix angle increases, while the leakage also increases. Comparison with a honeycomb stator seal shows that the helically grooved seals do much better with low inlet pre-swirl flow but no better than honeycomb stator seals for high fluid prerotation. However, there is clearly a penalty in leakage for the helically grooved seal.

Hence, the authors suggest that helically grooved seals should be used with a swirl brake for optimum effectiveness. Anti-swirl brakes are another effective device to enhance rotordynamic stability (Childs and Ramsey, 1990). Since the pre-swirl velocity is reduced or eliminated by a swirl brake, the magnitude of the cross-coupled stiffness becomes very small, and thereby the rotordynamic stability is significantly improved.

Murphy and Vance (1980) extend *Aljord's theory* (Alford, 1965) to a multi-bladed labyrinth seal while neglecting the circumferential flow within the labyrinth seal. The model predicts a significant equivalent damping coefficient in a seal with a diverging clearance configuration along the axial flow direction. Vance, et al. (1993) conduct extensive coast-down experiments to evaluate the equivalent damping characteristics of labyrinth seals. Both teeth-on-stator and teeth-on-rotor gas seals have been tested with different clearance configurations. However, the experimental results demonstrate that the direct damping from various types of labyrinth gas seals is generally very small. The authors reason that the predicted large pressure variations around the continuous annular groove of a labyrinth seal can not exist due to the circumferential swirl flow.

Vance, et al.(1993) introduce a gas pocket damper for high temperature applications as a replacement for conventional squeeze film dampers. A theoretical model is also developed for compressible fluid dampers. The dynamic pressure in a pocket can be out of phase with the vibratory motion since the flow of a gas into and out of the pocket is regulated by the vibratory motion. Therefore a gas pocket may work like an ideal damper element. The main idea is to find a configuration in which the dynamic force due to the pocket pressure acts on the whirling journal opposing the vibratory velocity. The isentropic flow model without viscous effects predicts the dynamic force coefficients to be strongly dependent on the excitation frequency. The damping coefficients are proportional to the supply pressure. The theory also predicts that the characteristic of damping is determined by the dynamic variation of the ratio of inlet area to exit area. Sundararajan and Vance (1995) confirm experimentally that a single pocket gas damper can provide a maximum damping of 13.2 lb-sec/in at an excitation frequency of 100 Hz.

Vance and Schultz (1993) introduce a novel type of gas damper seals, namely a

TAMSEAL™, and derived from the teeth on stator labyrinth seal by using the same mechanism as in the gas pocket damper. The gas damper seal can be used in any turbomachine with compressible working fluids and offers two distinct features that are critical to provide damping. The first one is that the radial rotor to blade clearances must diverge in the axial flow direction in the seal. Secondly, partition walls divide the annular circumferential groove of the labyrinth seal into several pockets. This design greatly reduces the velocity of the circumferential bulk-flow in the seal cavities. Vance and Li (1996) investigate the rotordynamic characteristics of a two-bladed gas damper seal by coast down and rap tests. Comparisons with a conventional labyrinth seal show that the gas damper seal has much higher damping than a conventional labyrinth seal of the same dimensions. Therefore, the gas damper seal has potentially wider use to suppress rotor synchronous vibrations since severe imbalance is a recurring problem in super-critical machinery. Tests also show that the leakage rate of the gas damper seal is about 30% larger than that of a conventional labyrinth seal with the same dimensions. Li and Vance (1995) study experimentally the effects of the clearance ratio and the number of teeth on short gas damper seals. Test results demonstrate that the damping coefficient decreases with the decrease in clearance ratio and the increase in the number of teeth. This novel type of gas damper seal has been installed in back-to-back industrial compressors to eliminate subsynchronous vibration effectively (Richards, et al., 1995).

Note that this novel damper seal, unlike other damping devices commonly used in turbomachinery, does not rely on the fluid viscosity to dissipate energy. So far a simplified theoretical analysis of the gas damper seal is available (Vance, et al., 1993, Vance and Sundararajan, 1993). The current model only accounts for axial flow continuity, neglects the effects of the fluid viscosity and the circumferential fluid swirl in the seal cavity, and assumes a uniform pressure distribution along the circumferential direction. Although the model can predict both direct stiffness and damping coefficients with limited accuracy, it can not provide values of the cross-coupled dynamic force coefficients. Therefore, a more complete computational model is needed to account for more practical operation conditions, and include the effects of circumferential flow and fluid viscosity.

## A BULK-FLOW MODEL OF GAS DAMPER SEALS

The gas damper seal is derived from the teeth-on stator labyrinth seal, and a typical two-bladed gas damper seal is shown in Figure 1. The teeth radial clearance increases in the axial flow direction. The circumferential grooves in the seal are divided into several identical cavities by the partition walls. The flow fields in the seal cavities are determined by the upstream flow conditions and the circumferential flow across the gap between the tip of the partition wall and the rotor surface. The pre-swirl of fluid and the rotor speed may induce a strong circumferential flow in the seal. Since the partition wall provides a wedge effect in the circumferential direction, the steady-state bulk-flow field in the gas damper seal varies periodically along the circumferential direction.

The fluid flow in the gas damper seal is generally fully turbulent due to the large axial pressure ratio across the seal, the high rotor surface speed, and the large seal clearances. In some circumstances, the axial pressure drop can be large enough to induce sonic flow conditions at the exit plane for a gas damper seal with few teeth.

### Governing equations

The bulk-flow theory of Hirs (Hirs, 1973) is used in this analysis. The viscous compressible fluid in the seal cavity is assumed as an isothermal ideal gas ($\rho = P/R_gT = P/V_*^2$), where $V_*$ is a characteristic velocity proportional to the fluid sonic speed. The pressure in the cavity is assumed as constant and varying only in the circumferential direction since the seal grooves are deep. The pressure drops across the seal teeth are given by empirical leakage formulae (Childs, 1993). The one control-volume bulk-flow model for a two-bladed gas damper seal is shown in Figure 2. For a gas damper seal divided into $N_c$ identical cavities of angular extent $2\beta = 2\pi/N_c$, the compressible bulk-flow in the seal cavity is characterized by the following continuity, circumferential momentum, and axial flow rate equations:

*Continuity equation*

$$\frac{1}{V_*^2}\left[\frac{\partial(PA)}{\partial t} + \frac{\partial(PAU)}{R_a\,\partial\theta}\right] + \zeta_r(\dot{M}_b - \dot{M}_z) = 0 \qquad (1)$$

*Circumferential momentum equation*

$$\frac{1}{V_*^2}\left[\frac{\partial(PAU)}{\partial t} + \frac{1}{R_a}\frac{\partial(PAU^2)}{\partial\theta}\right] + \zeta_r(\dot{M}_b U - \dot{M}_s U_s) = -\frac{A}{R_a}\frac{\partial P}{\partial\theta} + \Delta\tau_z \qquad (2)$$

where $\{A=(B+H)L\}$ is the cross-section area of the seal groove, and $H$ is the film thickness closest to the rotor.

*Axial leakage equation*

$$\begin{aligned} \dot{M} &= \frac{(\mu_c \mu_f H)}{V_*}\sqrt{P_u^2 - b_c P_d^2} \\ b_c &= 1.0 \quad (\textit{for unchoked flow}) \\ b_c &= 0.0 \quad (\textit{for choked flow}) \end{aligned} \qquad (3)$$

where $P_u$ and $P_d$ are the local upstream and downstream pressure across the teeth of the seal or the partition walls. Refer to the Nomenclature for a full description of all variables.

**Shear stress model**

Hirs bulk-flow theory and Moody's friction formulae have been successfully used for the dynamic analysis of turbulent flows in liquid bearings and seals, or gas seals (San Andres, 1990, 1993, Yang, et. al., 1993). In thin film flows, the shear stress difference $\Delta\tau_z$ combines the contributions of the shear stresses acted on both seal stator and rotor surfaces (Launder and Leschziner, 1978), and is defined as:

$$\Delta\tau_z = -\frac{\mu L}{D_h}\left[k_z U - k_f \frac{\Omega R_r}{2}\right] \qquad (4)$$

where $D_h$ is the seal hydraulic diameter typically defined as $\{2L(B_s+H_s)/(L+B_s+H_s)\}$ for a two-bladed gas damper seal. The shear stress parameters $k_z$ and $k_f$ are expressed as:

$$\begin{aligned} k_f &= \zeta_r k_r \\ k_z &= \frac{\zeta_r k_r}{2} + \frac{(\zeta_s L + B_s + B_b)}{2L} k_s \end{aligned} \qquad (5)$$

where $L$ is the pitch length of the seal, $B_a$ and $B_b$ are the heights of the upstream and downstream teeth of the seal, respectively. $\zeta_r$ and $\zeta_s$ are the ratios of the rotor radius and the seal outside radius to the average radius of the seal. $k_s$ and $k_r$ are turbulent shear stress parameters which are functions of the local Reynolds numbers and the Moody's friction factors at the stator and rotor surfaces, i.e.

$$k_s = f_s Re_s = f_s \left[ \frac{\rho D_h}{\mu} \sqrt{U^2 + W^2} \right]$$
$$k_r = f_r Re_r = f_r \left[ \frac{\rho D_h}{\mu} \sqrt{(U - \Omega R_r)^2 + W^2} \right] \qquad (6)$$

where the local Reynolds numbers $Re_r$, $Re_s$ and the Moody's friction factors $f_r$, $f_s$ at the stator and rotor surfaces are given in the Nomenclature.

**Boundary conditions**

Uniform supply pressure and back pressure fields are assumed at the inlet and exit places of the seal as determined by the operation conditions. A uniform inlet pre-swirl ratio is adopted as well, i.e $\alpha_{in} = U_s/\Omega r_r$. In a centered gas damper seal with several identical circumferential cavities, the zeroth-order solution for just one cavity is needed, since by symmetry other cavities have identical steady-state pressure and mean circumferential velocity fields. Therefore, the pressure and velocity at the partition wall should be specified as boundary conditions as shown in Figure 1.

a) A pressure difference exists at the partition wall due to the local acceleration of the flow from the upstream cavity to the downstream cavity. An expression of the pressure at the partition wall of infinitesimal thickness is given as:

$$P(\beta) = P_d \left[ 1 - \xi_w \left( \frac{\Delta P}{P_d} \right)^2 \right] \qquad (7)$$

where $\xi_w$ is an empirical coefficient accounting for the effect of the gap between the rotor surface and the tip of the partition wall, $\Delta P$ is the pressure drop across the partition wall

and $P_d$ is the local downstream pressure.

b) The circumferential velocity of the flow at the partition wall consists of three components due to the rotor surface speed, the upstream pre-swirl, and the pressure drop across the partition wall, respectively, i.e.

$$U(\beta) = \alpha_r\left(\frac{\Omega R_r}{2}\right) + \alpha_s U_s + \alpha_w\left(\frac{\dot{M}_w}{\rho_w H_w}\right) \tag{8}$$

where $\dot{M}_w$ is the circumferential mass flow across the partition wall driven by the pressure drop across the wall, $\rho_w$ and $H_w$ are the gas density and the clearance at the partition wall respectively. $U_s$ is the upstream pre-swirl velocity. Note that $\alpha_r$, $\alpha_s$ and $\alpha_w$ in the equation above correspond to empirical factors which should satisfy the requirements of the conventional labyrinth seal if the partition walls are removed from the seal groove.

c) For a centered gas damper seal with identical circumferential cavities, the following relations between the cavities exist at the steady-state conditions:

$$\begin{aligned} P^i(\theta + 2\beta) &= P^1(\theta) \\ U^i(\theta + 2\beta) &= U^1(\theta) \\ \textit{with} \quad -\beta \le \theta &\ge \beta \end{aligned} \tag{9}$$

where the superscript i denotes the i-th pocket.

**Zeroth-order and first-order perturbation equations**

A perturbation analysis of the compressible bulk-flow equations is performed to evaluate the dynamic force coefficients of the gas damper seal. Assume that the rotor whirls at frequency ($\omega$) with small amplitude motion ($e$) about the seal concentric position. In general, the seal clearance is represented by the following equations:

$$\begin{aligned} H &= H_0 + e_j H_j e^{i\omega t}, \qquad i = \sqrt{-1}, \\ H_X &= \cos\theta, \qquad H_Y = \sin\theta \end{aligned} \tag{10}$$

where $H_0$ is the static seal clearance for a centered rotor. For small amplitude motions, all flow variables can be expressed as the superposition of the steady-state and first-order dynamic fields. In general,

$$\Phi = \Phi_0 + e_j \Phi_j e^{i\omega t}, \qquad \Phi = U, W, P, k_x, k_y, Re_r, Re_z, \ldots, etc. \tag{11}$$

Substituting the perturbed variables into the governing equations (1), (2), and expanding these equations yields the zeroth-order and first-order governing equations.

*Zeroth-order continuity equation*

$$\frac{1}{V_*^2}\frac{\partial(P_0 A_0 U_0)}{R_a \partial\theta} + \zeta_r(\dot{M}_{b0} - \dot{M}_{z0}) = 0 \tag{12}$$

*Zeroth-order circumferential momentum equation*

$$\frac{1}{V_*^2}\frac{\partial(P_0 A_0 U_0^2)}{R_a \partial\theta} + \zeta_r(\dot{M}_{b0} U_0 - \dot{M}_{z0} U_{z0}) = -\frac{A_0}{R_a}\frac{\partial P_0}{\partial\theta} + \Delta\tau_{z0} \tag{13}$$

*Zeroth-order axial leakage equation*

$$\dot{M}_0 = \frac{(\mu_c \mu_f H)_0}{V_*}\sqrt{P_{u0}^2 - b_c P_{d0}^2} \tag{14}$$

The boundary conditions for the zeroth-order governing equations at the partition wall are the same as those given by equations (8) and (9).

*First-order continuity equation*

$$\frac{i\omega}{V_*^2}[P_0 L H_j + A_0 P_j] + \frac{1}{R_a V_*^2}\frac{\partial}{\partial\theta}[P_0 A_0 U_j + P_0 U_0 L H_j + U_0 A_0 P_j] + \eta_{mh} H_j + \eta_{mp} P_j = 0 \tag{15}$$

*First-order circumferential momentum equation*

$$\frac{i\omega}{V_*^2}[P_0 A_0 U_j] + \frac{1}{R_a V_*^2}\frac{\partial}{\partial\theta}[P_0 U_0 U_0 U_j] - \frac{1}{R_a V_*^2}[P_0 A_0 U_j + P_0 U_0 L H_j + A_0 U_0 P_j]\frac{\partial U_0}{\partial\theta} = -\frac{A_0}{R_a}\frac{\partial P_j}{\partial\theta} + C_{xu}U_j + C_{xh}H_j + C_{xp}P_j \tag{16}$$

where

$$\begin{aligned} C_{xu} &= \eta_{xu} - \eta_{uu} \\ C_{xh} &= \eta_{xh} - \eta_{uh} + \eta_{mh}U_0 + \frac{L}{R_a}\frac{\partial P_0}{\partial\theta} \\ C_{xh} &= \eta_{xp} - \eta_{up} + \eta_{mp}U_0 \end{aligned} \tag{17}$$

*First-order axial leakage equation*

$$\dot{M}_j = \eta_h H_j + \eta_{pu} P_{uj} + \eta_{pd} P_{dj} \tag{18}$$

where the subscript "j" (= X, Y) denote the directions of perturbation for the first-order variables. The $\eta$ coefficients arise from the perturbation of the empirical axial leakage terms and turbulent shear stress terms. Since the inlet pre-swirl velocity, the supply pressure and the back pressure of the seal are regarded as invariant, the boundary conditions for the first-order governing equations are given as follows:

at the seal inlet: $$P_{xj} = 0, \qquad U_{xj} = 0 \tag{19}$$

at the seal outlet: $$P_{bj} = 0 \tag{20}$$

at the partition wall: $$P_j(\beta) = \beta_{jpu} P_{uj} + \beta_{jpd} P_{dj} \tag{21}$$

$$U_j(\beta) = \alpha_{jh} H_j + \alpha_{jpu} P_{uj} + \alpha_{jpd} P_{dj} \tag{22}$$

where the $\beta_j$ and $\alpha_j$ coefficients arise from the first-order perturbation of the boundary conditions at the partition wall.

**Numerical method of solution**

Zeroth-order and first-order discretizatized algebraic equations are derived using the SIMPLEC finite-difference scheme of Van Doormal and Raithby (1984). The flow field is represented by a series of discrete nodal pressures and circumferential velocities on staggered grids (Patankar, 1980). The upwinding scheme is implemented for both the zeroth-order and first-order advection terms in order to make the algorithm more stable.

Both the steady-state and first-order flow fields are numerically calculated based on an iterative procedure. The empirical leakage equation is used to guess an initial uniform pressure field within the seal. The velocity components are first calculated from the circumferential momentum equation using the guessed pressure field, and then a pressure correction equation based on the continuity equation provides corrected pressure and velocity fields. The updated pressure and velocity fields are substituted into the momentum and pressure correction equations again resulting in generally more accurate velocity and pressure field solutions. The iterative procedure above is repeated until the following convergent criteria for the mass flow and pressures are satisfied.

a) For the steady-state solution, the ratio of the global mass flow source to the total mass flow of the seal is required to be less than $1\times10^{-6}$. On the other hand, the maximum difference between two consecutive iterations for the pressure field should be less then $1\times10^{-6}$ of the inlet pressure.

b) For the solution of the first-order linear equations, the process continues until the solution converges to within a bound of $1\times10^{-7}$ of the inlet pressure in the differences between two consecutive iterations for the modulus of the first-order complex pressure field.

**Seal dynamic forces and force coefficients**

The zeroth-order solution determines the steady-state cavity pressure and circumferential velocity as well as the seal axial leakage. The first-order solution leads to the determination of the dynamic force characteristics of the gas damper seal. The dynamic forces of the seal are

calculated from the integration of the complex first-order pressure field ( $P_j$ ) over the journal surface:

$$F_i = LR_r \sum_{n=1}^{N_c} \int_{-\beta}^{\beta} P_j^n H_i \, d\theta \, e_j \, e^{(i\omega t)}; \qquad i, j = X, Y \tag{23}$$

According to the definition of the rotordynamic force coefficients (Lund, 1987), the stiffness and damping coefficients of the seal are evaluated by:

$$(K_{ij} + i\omega C_{ij}) = \frac{-F_i}{e_j \, e^{(i\omega t)}} = -LR_r \sum_{n=1}^{N_c} \int_{-\beta}^{\beta} P_j^n H_i \, d\theta; \qquad i, j = X, Y \tag{24}$$

For small amplitude motions around the concentric seal position, the direct force coefficients of the seal are symmetric and the cross-coupled coefficients of the seal are anti-symmetric, i.e.

$$\begin{aligned} K_{XX} &= K_{YY}, \qquad K_{XY} = -K_{YX} \\ C_{XX} &= C_{YY}, \qquad C_{XY} = -C_{YX} \end{aligned} \tag{25}$$

This relationship allows the first-order equations to be solved only in one direction (in this case the solution for a perturbation in the X direction is performed). It is noted that the seal dynamic force coefficients are dependent on the excitation frequency ($\omega$) for compressible fluids.

In actual experiments, the dynamic forces are much easier to measured directly. For a small amplitude circular motion around the centered seal position, the radial and tangential dynamic forces are constant, and defined in terms of the dynamic force coefficients as:

$$\begin{aligned} F_r &= -(K_{XX} + \omega C_{XY})e \\ F_t &= -(\omega C_{XX} - K_{XY})e \end{aligned} \tag{26}$$

according to the definitions above, a negative tangential force is stabilizing, while a negative

radial force is an inward (centering) force.

## VALIDATION OF THE BULK-FLOW MODEL

Validation of the bulk-flow model is discussed in the balance of this report. A computer program for analysis of two-bladed gas damper seals has been developed. Numerical predictions based on the analysis detailed earlier are presented in this section. Comparisons are made to experimental results and the predictions from the earlier model for a two-bladed gas damper seal (Li, 1995). To the authors knowledge, no experimental dynamic force coefficients are available for two-bladed teeth-on-stator gas labyrinth seals. Numerical results of the present bulk-flow model for a two-bladed labyrinth seal are compared to predictions from a two-control volume model ( Scharrer and Childs, 1988). Finally the dynamic performance of a typical two-bladed gas damper seal is discussed.

### Comparisons to existing test results for a two-bladed gas damper seal

Li (1995) evaluates the rotordynamic performance of a two-bladed gas damper seal by coast-down and rap tests. Therefore, comparisons of the current model to the earlier analysis of Vance et. al (1993) and experimental values for the direct damping coefficient of a gas damper seal are available. A description of the test rig, measurement procedure and test results is given by Li (1995). The test seal has four partition walls dividing the annular groove into four identical circumferential cavities. Axial mass flow rates are measured at room temperature (around 74 °F) and one atmosphere back pressure. Direct damping coefficients are identified from measurements of the logarithm decrement of the decaying free vibration waveforms at null rotor speed. The dimensions of the seal and operating conditions are shown in Table 1.

In the earlier simplified model, the flow discharge coefficients are regarded as constant, though they must be first adjusted by matching to the measured mass flow rate before useful predictions are obtained. Li (1995) determines a discharge coefficient equal to 0.90, whereas in the current bulk-flow model the variable flow coefficients are directly evaluated in the analysis. The frequency of the decaying free vibration of the test rotor is around 66 Hz, and thus an excitation frequency of 66 Hz is used as an input parameter for both the earlier and

current bulk-flow models.

Table 1. Two-bladed gas damper seal dimensions and operating conditions for rap tests ( Li, 1995)

| | |
|---|---|
| No. of seal teeth: | 2 |
| No. of circumferential pockets: | 4 |
| Overall seal length: | 1.000" (25.4 mm) |
| Blade thickness: | 0.125" (3.175 mm) |
| Inside pitch length: | 0.750" (19.05 mm) |
| Seal teeth height: | 0.176" (4.4704 mm) |
| Inner diameter (rotor): | 4.000" (101.6 mm) |
| Outer diameter (stator): | 4.360" (110.744 mm) |
| Inlet clearance: | 0.004" (0.1016 mm) |
| Exit clearance: | 0.008" (0.2032 mm) |
| Temperature of gas at inlet: | 74 °F ( 296 °K) |
| Molecular weight of gas: | 29 |
| Gas constant (lb-in/lbm-R): | 639.31034 (287 J/kg-K) |
| Inlet pressure, $P_s$ | 20-50 psia (1.38-3.45 bar) |
| Exit pressure, $P_b$ | 14.7 psia (1.013 bar) |
| Rotor speed: | 0.0 rpm |

The experimental results and theoretical predictions for seal leakage, direct damping and stiffness coefficients are compared. Figure 3 shows the mass flow rate to agree well with test results. Note that the theoretical predictions are within 12% of the test data accounting for 20% uncertainty in mass flow measurement. The earlier theory predicts mass flow rate more accurately than the current model for test conditions prior to flow choking at the seal exit. However, an adjusted flow discharge coefficient is used in the earlier model. The two models predict essentially the same mass flow rate after choking since an identical flow rate formula is adopted for choked flow.

Figure 4 shows the experimental and theoretical damping force coefficient as a function of the supply pressure at the seal inlet. Both theoretical models predict the direct damping coefficient $C_{XX}$ to increase with the inlet pressure. The earlier model largely overpredicts the damping coefficient especially at high inlet pressures since it neglects the circumferential flow within the seal. On the other hand, the current bulk-flow model predicts the damping coefficient

very well over the range of test inlet pressures.

Figure 5 illustrates that both theoretical models predict a negative direct stiffness for the two-bladed gas damper seal. This fact has been indirectly confirmed by coastdown tests in which the critical speed of the rotor-bearing s; em decreases with 'e supply pressure (Li, 1995). Although no test data of the direct stiffness coefficient is available for comparison, it is suspected that the earlier model also overpredicts the direct stiffness force coefficient.

**A numerical example of a two-bladed gas labyrinth seal**

Rotordynamic characteristics of a two-bladed gas labyrinth seal are evaluated for comparison to a two-control volume bulk-flow model (Scharrer 1988). This conventional gas labyrinth seal has the same geometric dimensions as the two-bladed gas damper seal given in Table 1 except for its see-through clearance configuration. The rotor and stator surfaces are regarded as smooth, and a rotor speed of 4,200 rpm is specified. Since synchronous whirl is of major concern in rotating machines, an excitation frequency of 70 Hz is used to calculate the seal dynamic force coefficients. The geometric dimensions of the gas labyrinth seal and operating conditions are given in Table 2.

Comparisons of predictions between the current model and the two-control volume model follow. Figure 6 shows both models to predict nearly identical mass flow rate and cavity pressure for a range of inlet pressures from 20 to 70 psia. There is a slight discrepancy in flow rates in the region near choking. The predicted circumferential velocity appears to be insensitive to the inlet pressure. The current model predicts a mean circumferential velocity 50% less than the two-control volume model because both models use different shear stress formulae. Note that the rotor spins with a surface velocity of 22.34 m/s.

Both computational models predict the same trends in the damping coefficients as the supply pressure increases as shown in Figure 7. The damping coefficients predicted by both models are nearly the same prior to the choking pressure. At higher inlet pressure the predictions diverge slightly. Both damping coefficients $\{C_{XX}, C_{XY}\}$ increase with inlet supply pressure. However, the direct damping coefficient of the labyrinth seal is very small and negligible compared to the damper seal case analyzed first.

Figure 8(a) shows the direct synchronous stiffness to be negative for all inlet pressures.

Table 2. A see-through two-teeth gas labyrinth seal dimensions and operating conditions for theoretical predictions

| | |
|---|---|
| No. of seal teeth: | 2 |
| Overall seal length: | 1.000" (25.4 mm) |
| Blade thickness: | 0.125" (3.175 mm) |
| Inside pitch length: | 0.750" (19.05 mm) |
| Seal teeth height: | 0.176" (4.4704 mm) |
| Inner diameter (rotor): | 4.000" (101.6 mm) |
| Outer diameter (stator): | 4.360" (110.744 mm) |
| Inlet clearance: | 0.004" (0.1016 mm) |
| Exit clearance: | 0.004" (0.1016 mm) |
| Temperature of gas at Inlet: | 75 °F ( 297 °K) |
| Gas constant (lb-in/lbm-R): | 639.31034 (287 J/kg-K) |
| Inlet pressure, $P_a$ | 20-70 psia (1.38-4.83 bar) |
| Exit pressure, $P_b$ | 14.7 psia (1.013 bar) |
| Rotor speed: | 4,200 rpm |
| Excitation frequency: | 70 Hz |
| Inlet pre-swirl ratio: | 0.5 |

The magnitude of the direct stiffness $K_{XX}$ increases slightly as the supply pressure increases. However, the direct stiffness sharply decreases above the pressure needed for choked flow. The current bulk-flow model predicts a smaller magnitude of the direct stiffness coefficient than the two-control volume bulk-flow model. In actual rotating machines, the effect of such small direct stiffness on the system rotordynamic performance is negligible compared to the shaft stiffness and the direct stiffness provided by the bearings.

The current model predicts positive cross-coupled stiffness coefficients $K_{XY}$ while the two-control volume model predicts negative values. Since there is no experimental data of the dynamic force coefficient for a two-teeth labyrinth seal, it is difficult to assert reasons explaining the difference in predictions.

**Comparisons to limited test data for a two-bladed see-through gas labyrinth seal**

Wright (1983) presents limited test results for the radial and tangential dynamic forces

of a two-teeth gas labyrinth on a subsynchronously whiling rotor. The effects of whirl direction, back pressure and pressure drop are investigated for limited conditions. Air is used as the working fluid in the test seal with a rotor spinning at 1,800 rpm. The seal back pressure varies from 15 psia to 60 psia, and the rotor is forced to whirl in a forward circular orbit with a subsynchronous whirl frequency at approximately one half of the rotor spinning frequency. Since the temperature and pre-swirl ratio of the working fluid are not explicitly given in the cited reference, a temperature of 74 °F and an inlet pre-swirl ratio equal to 0.5 are chosen as input parameters for the current model. The geometric dimensions of the seal and test conditions are shown in Table 3.

Experimental and theoretical comparisons for the mass flow rate and dynamic forces of the see-through two-teeth gas labyrinth seal are presented as follows. Figure 9 illustrates the current model to predict well the mass flow rate for the two back pressures. The discrepancies are less than 10% of the measured mass flow rate. Figure 10 shows the tangential force ($-F_t/e$) as a stabilizing force able to suppress rotor vibration. The magnitude of this force is

Table 3. A see-through two-teeth gas labyrinth seal dimensions and operating conditions (Wright, 1983)

| | |
|---|---|
| No. of seal teeth: | 2 |
| Overall seal length: | 0.6186" (15.712 mm) |
| Blade thickness: | 0.055" (1.397 mm) |
| Inside pitch length: | 0.5086" (12.918 mm) |
| Seal tooth height: | 0.198" (5.0305 mm) |
| Inner diameter (rotor): | 8.000" (203.2 mm) |
| Outer diameter (stator): | 4.360" (110.744 mm) |
| Inlet clearance: | 0.00624" (0.1585 mm) |
| Exit clearance: | 0.00624" (0.1585 mm) |
| Temperature of working gas : | 74 °F ( 296 °K) |
| Gas constant (lb-in/lbm-R): | 639.31034 (287 J/kg-K) (air) |
| Exit pressure, $P_b$ | 15, 30, 45 psia |
| Pressure drop: | 1 - 5 psi |
| Rotor speed: | 1,800 rpm |
| Whirl frequency: | 13.43 - 15.09 Hz |

proportional to the pressure drop. The current model underpredicts the seal tangential force, except for the case with the smallest pressure drop equal to 1 psi. Note that the predicted tangential force increases at a lower rate than the test tangential force.

The current model predicts poorly the radial dynamic force ($-F_r/e$) of the two-teeth gas labyrinth as shown in Figure 11. The test results show that the magnitude of the radial force is a positive centering force and nearly insensitive to the back pressure. The theoretical model grossly underpredicts the radial force as negative for the back pressure of 45 psia, and positive for the back pressure of 15 psia . On the other hand, the model severely underpredicts the magnitude of the radial dynamic force compared with the test results. Note that the pressure differences are very small for both back pressures. The Reynolds numbers in the tests changes from 520 to 2049. The seal forces are measured in laminar or transition flow regimes. However, the current model is developed based on the assumption of fully turbulent flow.

## DYNAMIC PERFORMANCE OF A TWO-BLADED GAS DAMPER SEAL

Numerous predictions for the rotordynamic characteristics of a two-bladed gas damper seal are obtained with the current bulk-flow computational program. The reference two-bladed gas damper seal geometry is given in Table 1. The effects of several important parameters on the rotordynamic force coefficients and dynamic forces are investigated. Theses parameters are the feed pressure at the seal entrance, the rotor speed, the preswirl velocity ratio and the excitation frequency. The dynamic performance of the gas damper seal with two types of exit clearances are compared to evaluate the feasibility of a hybrid brush/gas damper seal with controlled leakage. One type of exit clearance is that due to modulation by the shaft vibration, and another type of exit clearance is fixed as in a brush seal. In the following Figures, the notation *1X* indicates synchronous whirl, *0.5X* indicates subsynchronous whirl at a frequency equal to one half of the rotational speed, and *2X* indicates supersynchronous whirl at twice the rotational speed.

### The effect of the rotor speed on the dynamic force coefficients

Figure 12 shows the rotordynamic coefficients of the two-bladed gas damper seal as the

rotational speed increases from 1,000 rpm to 15,000 rpm. In all cases, the direct stiffness coefficient ($K_{XX}$) is negative, and its magnitude decreases with an increase in the rotor speed. On the other hand, the direct damping coefficient ($C_{XX}$) is positive, and decreases with increases in the rotor speed and whirl frequency. The cross-coupled stiffness coefficient ($K_{XY}$) is positive, first increases and then gradually decreases with the rotor speed. There is a maximum cross-coupled stiffness coefficient for each type of rotor whirl, always occuring at a fixed excitation frequency of 67 Hz. The cross-coupled damping ($C_{XY}$) follows a similar trend as the cross-coupled stiffness. Typically, the gas damper seal provides the larger dynamic force coefficients for rotor whirl at the lowest excitation frequencies for a specified shaft speed.

**The effect of the pre-swirl velocity on the dynamic force coefficients**

Figure 13 shows the rotordynamic force coefficients of the two-bladed gas damper seal versus the pre-swirl ratio at a fixed rotational speed of 9,000 rpm. Like other common labyrinth seals, the direct force coefficients are insensitive to the pre-swirl ratio while the cross-coupled coefficients linearly increase with the pre-swirl ratio. The direct stiffness coefficient ($K_{XX}$) and the cross-coupled damping coefficient ($C_{XY}$) are still negative, and the cross-coupled stiffness coefficient ($K_{XY}$) and the direct damping coefficient ($C_{XX}$) are positive. The cross-coupled force coefficients increase at the largest rate for the subsynchronous whirl ($0.5X$) in the three types of rotor whirl.

**The effect of the supply pressure on the dynamic force coefficients**

As shown in Figure 14, the supply pressure at the seal entrance has a significant effect on the dynamic force performance of the studied gas damper seal. For all cases the magnitude of the direct and cross-coupled damping coefficients increases with the supply pressure monotonically, changing their growth rates when the gas flow chokes at the seal exit. For subsynchronous whirl, the direct and cross-coupled stiffness coefficients follow the same trend. However for synchronous and supersynchronous whirls, the direct and cross-coupled stiffness coefficients decreases slightly when the gas flow is choked at the seal exit, and then continue to raise with the supply pressure. The dynamic force coefficients for subsynchronous whirl are more sensitive to the supply pressure than the other two types of rotor whirls.

**The effect of the excitation frequency on the dynamic forces**

The effects of the whirl frequency on the dynamic forces are evaluated for a fixed rotor speed of 9,000 rpm. A dimensionless excitation frequency is defined as the ratio of the excitation angular frequency to the rotational angular frequency ($\omega/\Omega$). Note that here the radial dynamic and tangential dynamic forces are shown in terms of $(-F_r/e)$ and $(-F_t/e)$, respectively. Figure 15 shows the dynamic forces are insensitive to the pre-swirl ratio. The radial force is positive and decreases sharply for excitation frequency ratios less than 1.5. For excitation frequency ratios greater than 2, the radial force levels off to a very small magnitude with a negative value. The tangential dynamic force is a stabilizing force, first increases with the excitation frequency, and after reaching its maximum at about a frequency ratio equal to 1.0, decreases rapidly.

As shown in Figure 16, the supply pressure has a more significant effect on the radial force for subsynchronous whirl compared to supersychronous whirl. For the synchronous whirl (the excitation frequency ratio equals one), the radial force has the same value for both supply pressures. On the other hand, the effect of the supply pressure on the tangential force is most significant around an excitation frequency ratio equal to unit. For this gas damper seal and specified conditions, increasing the supply pressure generates a large stabilizing force able to suppress synchronous vibration more effectively.

**The effects of the modulated vs. fixed exit clearance on the dynamic performance**

Figure 17 shows the rotordynamic force coefficients to follow identical trends for both types of exit clearances. The gas damper seal with a fixed exit clearance like in a brush seal has larger direct stiffness and damping coefficients. Furthermore, the gas damper seal with a fixed exit clearance has a lower (positive) cross-coupled stiffness than the gas damper seal with a modulated exit clearance.

Figure 18 shows the gas damper seal with a fixed exit clearance to introduce a larger positive radial force. On the other hand, the gas damper seal with a fixed exit clearance provides a much larger stabilizing force. From a rotordynamics point of view, the gas damper seal with a fixed exit clearance as in a brush seal provides more stability than the gas damper seal with a

modulated exit clearance.

## CONCLUSIONS

A numerical analysis for calculation of the rotordynamic force characteristics of a novel gas damper seal is presented. The one control-volume bulk-flow model is more complete than the earlier simplified model since it accounts for the effects of fluid viscosity and circumferential flow in the seal cavity. The nonlinear turbulent bulk-flow governing equations are solved for isothermal flow conditions. A perturbation method is used for calculation of the zeroth and first-order flow solutions determining the seal steady-state and dynamic force characteristics. The model can be applied to evaluate the dynamic force coefficients for gas labyrinth seals with any type of clearance configurations, such as see-through, converging and diverging configurations.

Comparisons to limited measurements for a two-bladed, four pocket gas damper seal show the current model to predict well the mass flow rate and the direct damping coefficient, and also a negative direct stiffness. The current model also provides comparable rotordynamic coefficients for a reference two-bladed gas labyrinth seal when compared to a two control-volume bulk-flow model. Typically, the dynamic force coefficients of the gas damper seal are much larger than those of the labyrinth seal with the same geometric dimensions. However the accuracy of the model to predict stiffness coefficients remains to be verified by experiments.

A parametric investigation conducted for a reference two-bladed, four pocket gas damper seal does provides insight into the rotordynamic characteristics of the novel gas damper seal. The dynamic force coefficients depend strongly on the rotor speed and the pressure drop across the seal. The magnitudes of the dynamic force coefficients decrease with increases in the rotor whirl frequency. The direct dynamic force coefficients are insensitive to the inlet pre-swirl velocity while the cross-coupled dynamic force coefficients are proportional to the inlet pre-swirl. However, the actual radial and tangential forces are almost independent of the inlet pre-swirl velocity since the direct stiffness and the direct damping coefficients are dominant in the gas damper seal. The gas damper seal provides the maximum stabilizing tangential force at certain operating conditions. Therefore, the current bulk-flow model is useful for optimizing

the dynamic performance of gas damper seals in actual applications..

The model predicts the gas damper seal with a fixed exit clearance as in brush seals to provide around 100% larger (stabilizing) tangential force than the conventional gas damper seal in which the exit clearance is modulated by rotor vibration. This indicates a hybrid brush/gas damper seal with controlled leakage at its exit to be of potential benefit in turbomachinery.

## ACKNOWLEDGMENTS

The support of the State of Texas Advanced Technology Program is gratefully acknowledged.

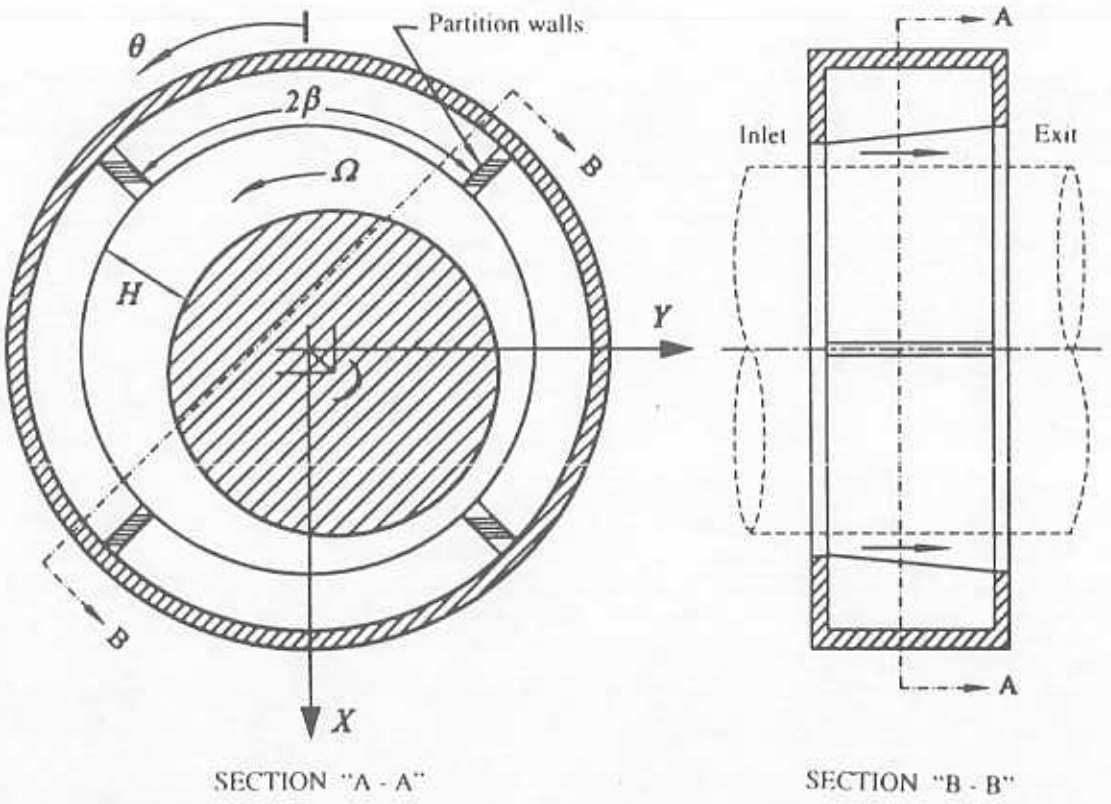


**Fig. 1 Schematic of a two-bladed gas damper seal with four partition walls**

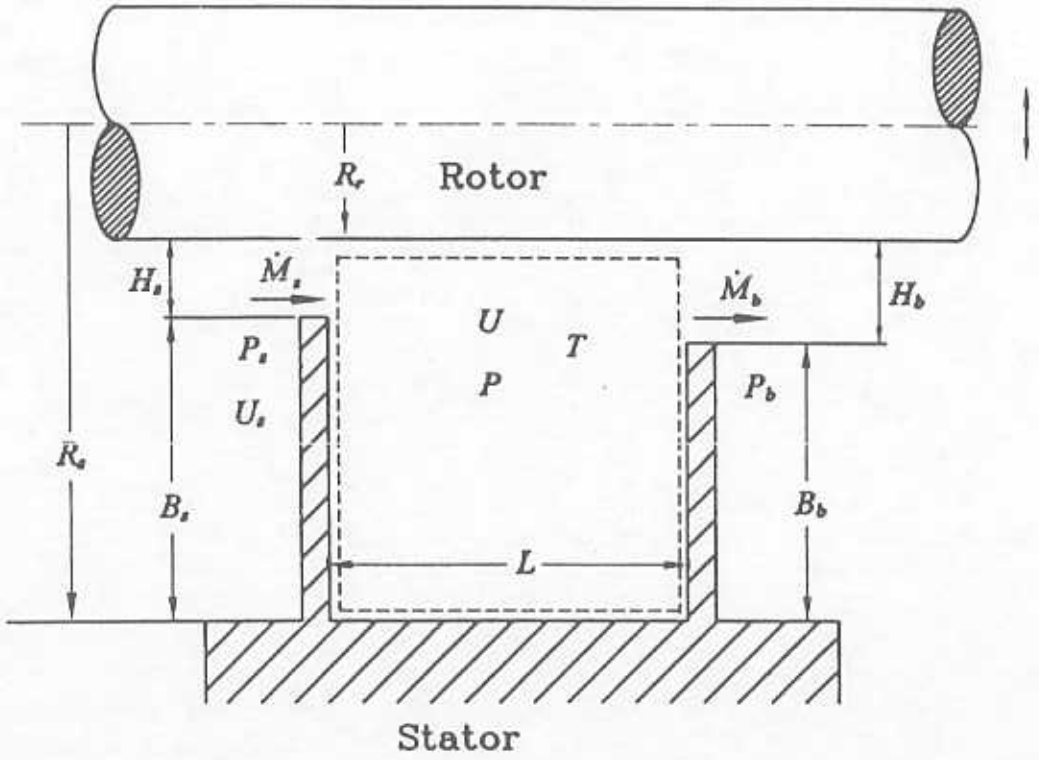


**Fig. 2 One control volume model for gas damper seals**

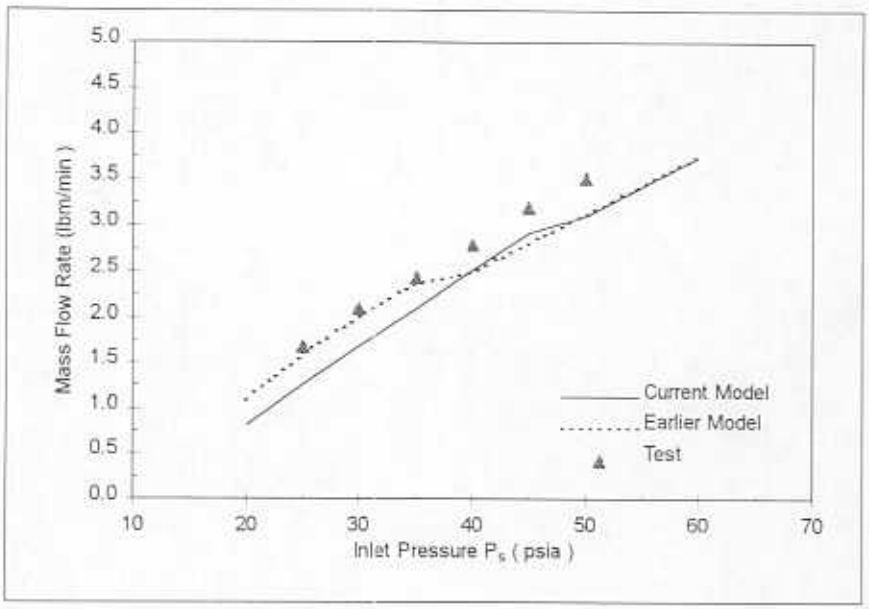


**Fig. 3 Experimental values and computed predictions of mass flow rates for a two-bladed gas damper seal vs. inlet pressure**

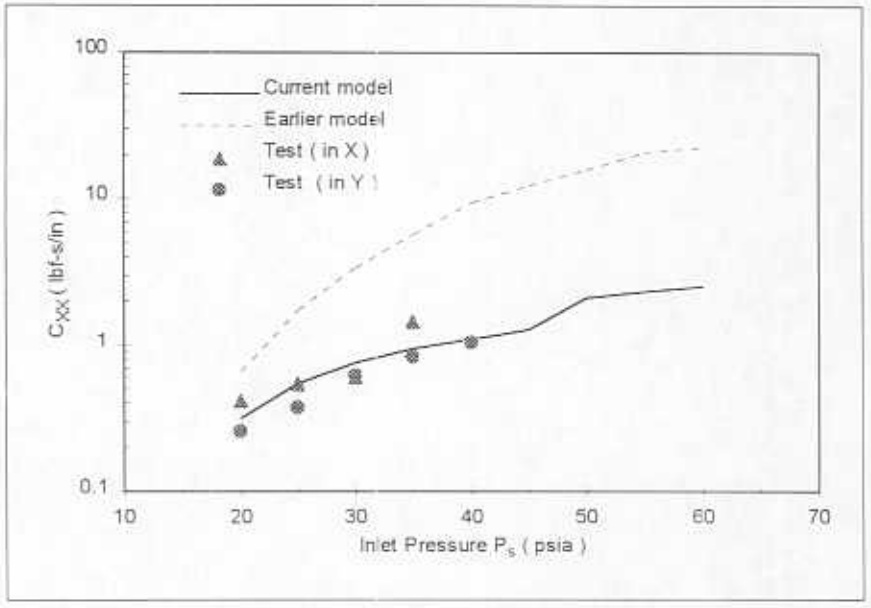


**Fig. 4 Experimental values and computed predictions for direct damping coefficients of a two-bladed gas damper seal ($\Omega$=0.0 rpm, $\omega$=66 Hz)**

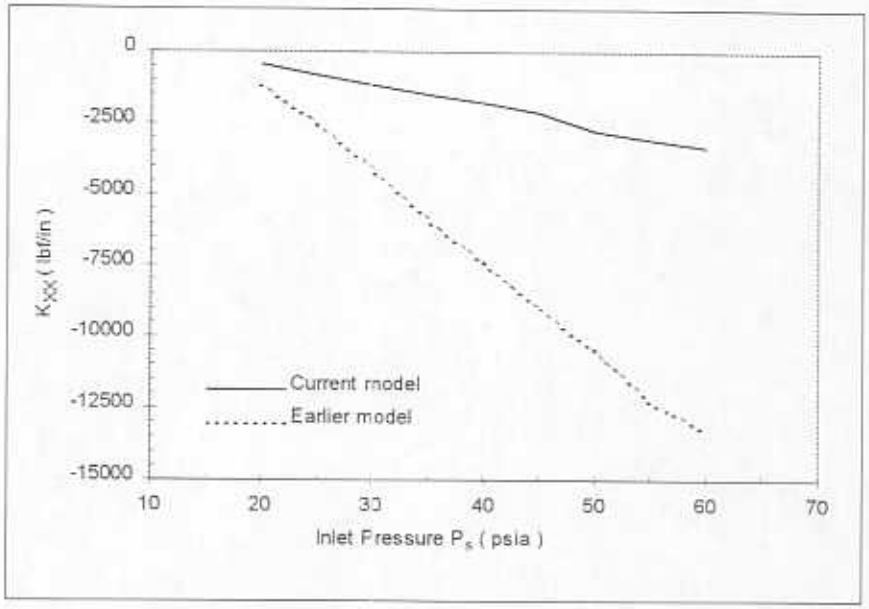


**Fig. 5 Computed predictions for direct stiffness coefficients of a two-bladed gas damper seal**
**( $\Omega$ = 0.0 rpm, $\omega$ = 66 Hz )**

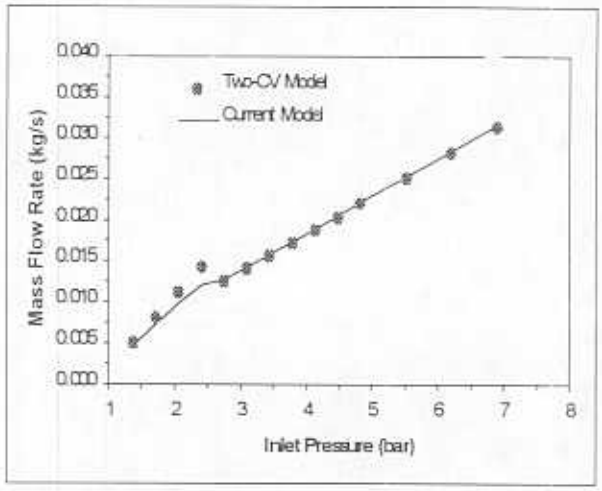


( a )

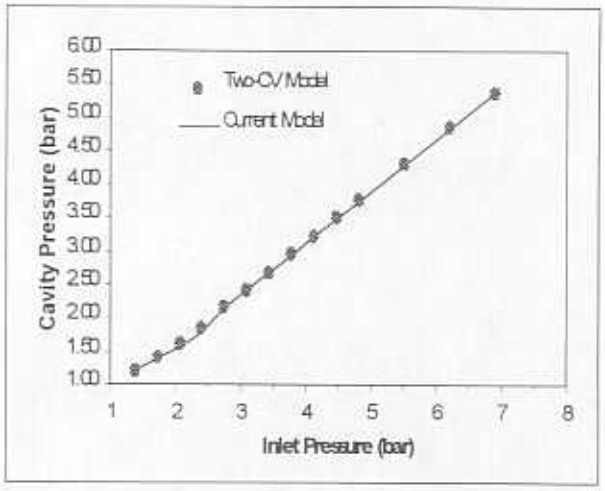


( b )

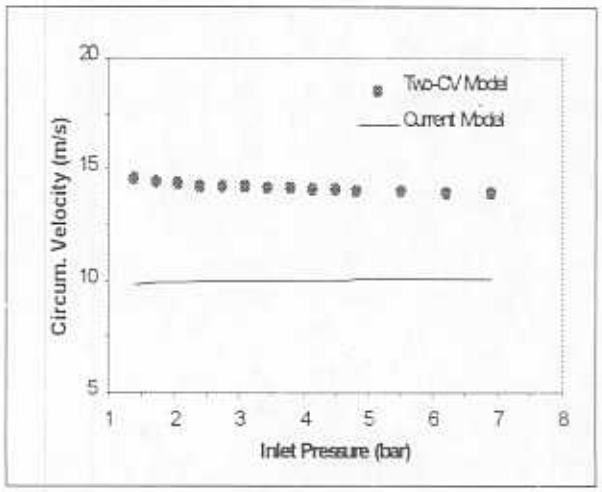


( c )

Fig. 6 Static characteristics of a two-teeth labyrinth seal vs. inlet pressure
( exit pressure = 1.013 bar, $\Omega$ = 4200 rpm, $\omega$ = 70 Hz )
(a) mass flow rate, (b) cavity pressure, (c) mean circumferential velocity

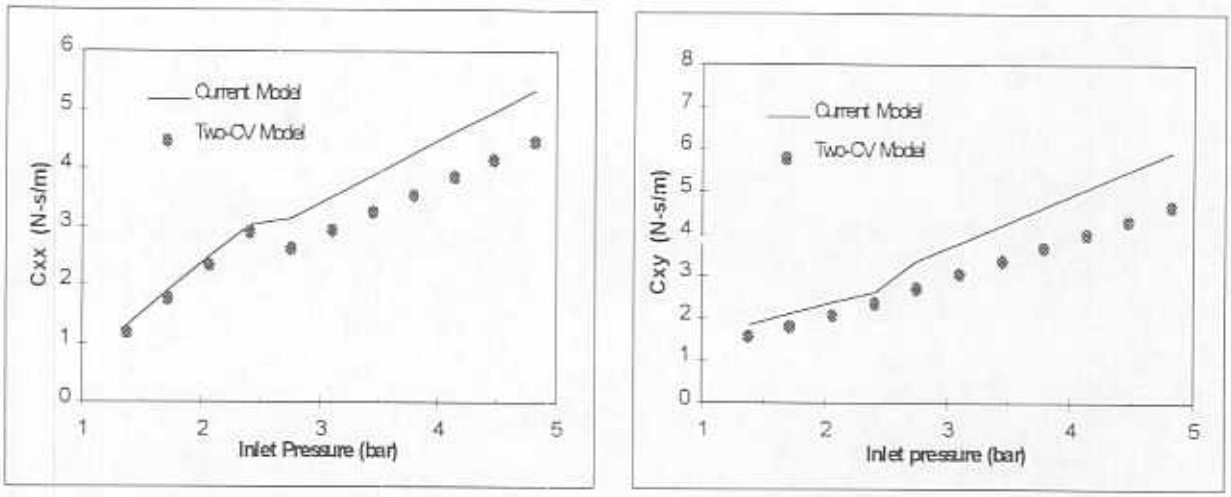


( a ) ( b )

Fig. 7 Damping coefficients of a two-teeth labyrinth seal vs. inlet pressure
( exit pressure = 1.013 bar, $\Omega$ = 4200 rpm, $\omega$ = 70 Hz )

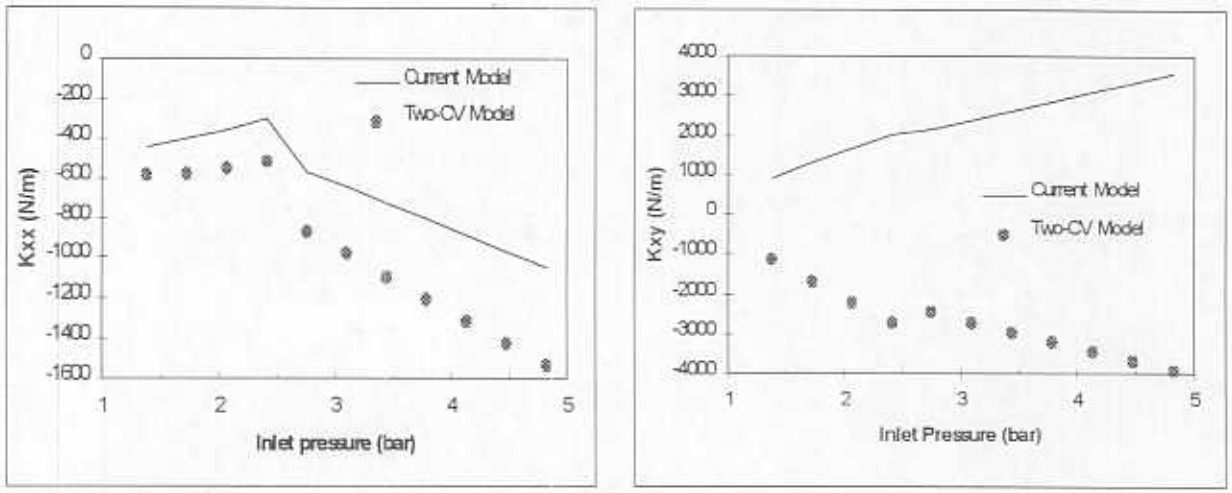


( a ) ( b )

Fig. 8 Stiffness coefficients of a two-teeth labyrinth seal vs. inlet pressure
( exit pressure = 1.013 bar, $\Omega$ = 4200 rpm, $\omega$ = 70 Hz )

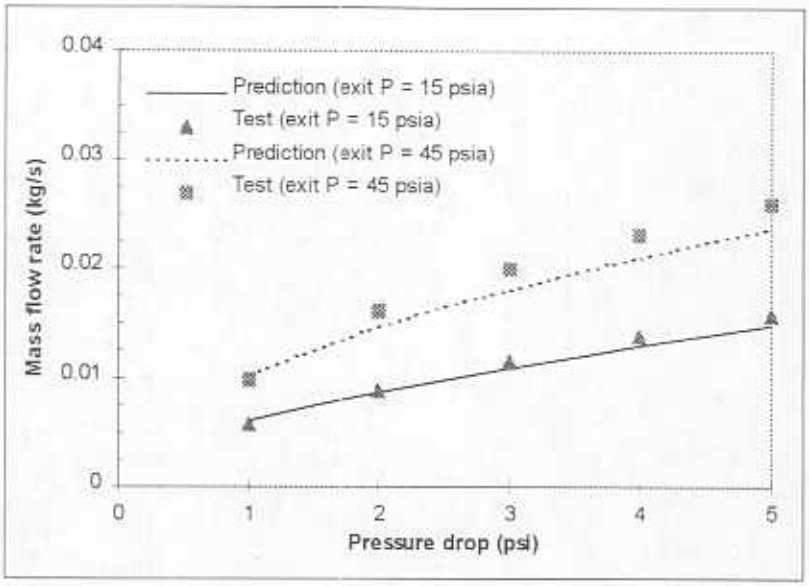


Fig. 9 Experimental and theoretical mass flow rates for a see-through labyrinth seal at two back pressures (Wright, 1983)

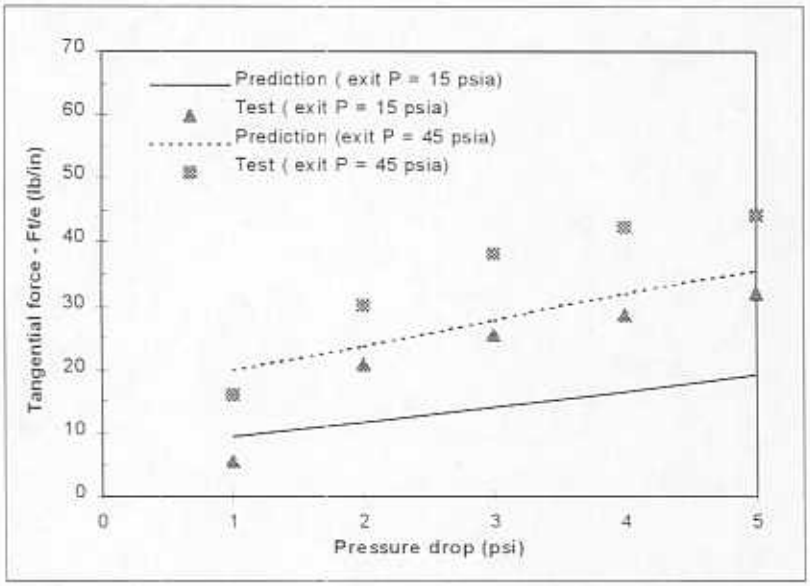


Fig. 10 Experimental and theoretical tangential dynamic forces for a see-through labyrinth seal at two back pressures (Wright, 1983)

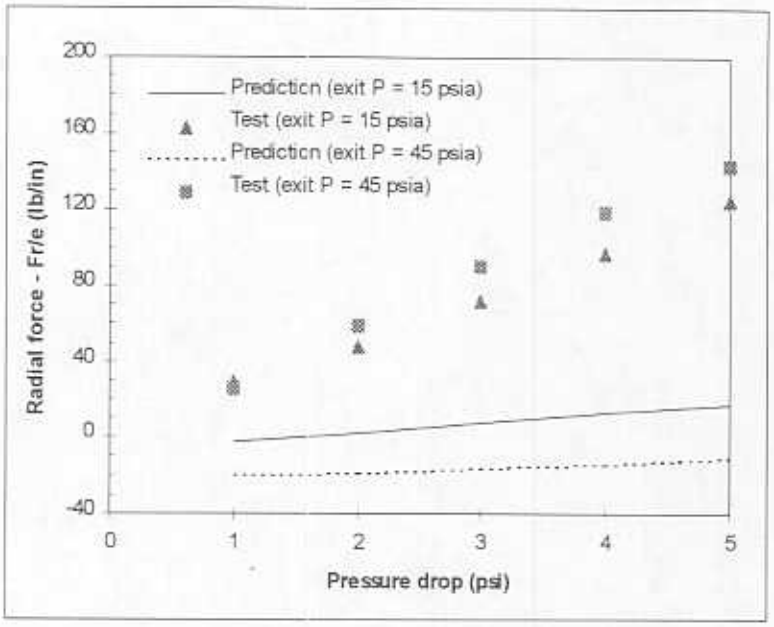


Fig. 11 Experimental and theoretical radial dynamic forces for a see-through labyrinth seal at two back pressures (Wright, 1983)

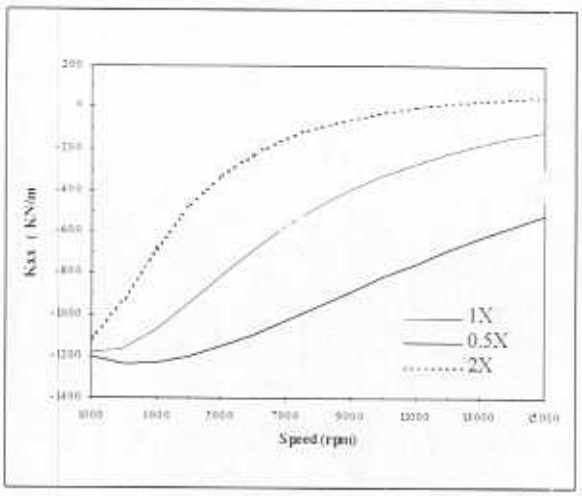


(a)

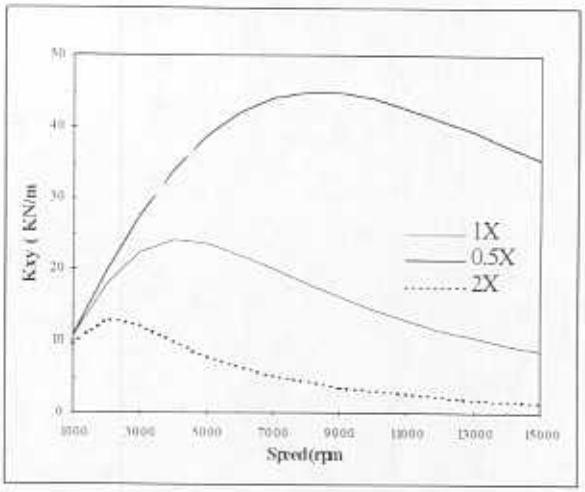


(b)

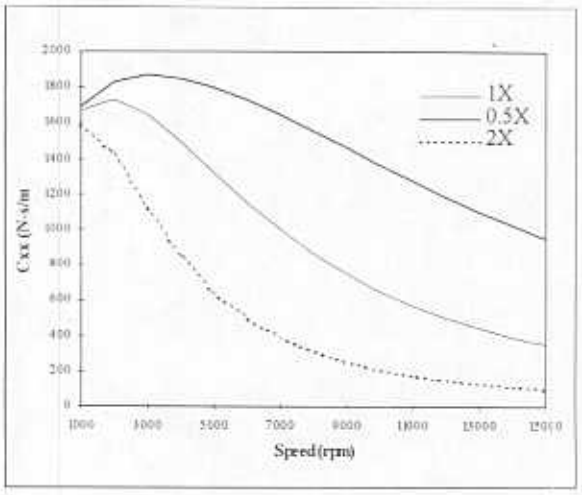


(c)

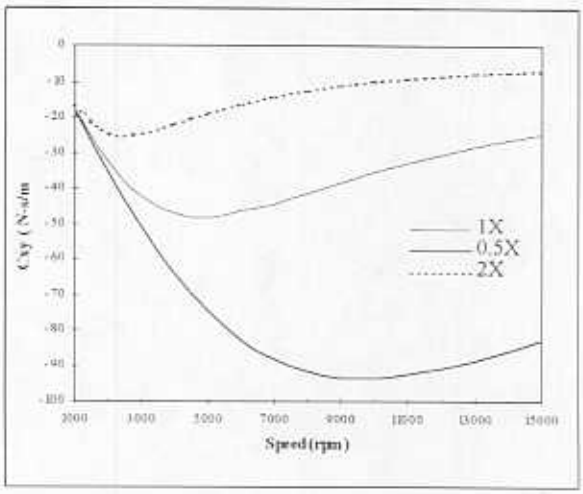


(d)

**Fig. 12 Dynamic force coefficients of a two-bladed gas damper seal vs. rotor speed ( inlet pressure=4.1347 bar, exit pressure=1.013 bar, pre-swirl ratio=0.0 )**

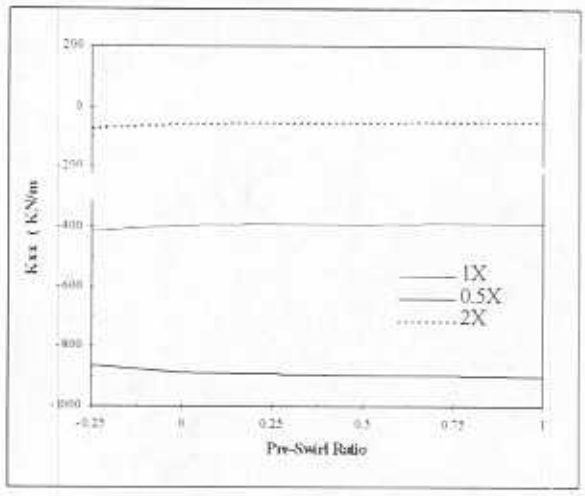


(a)

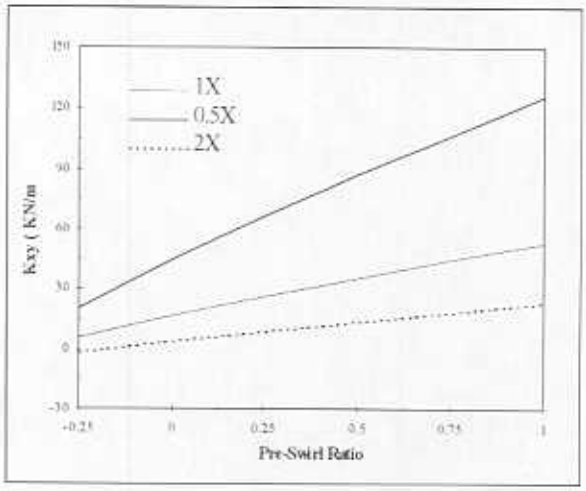


(b)

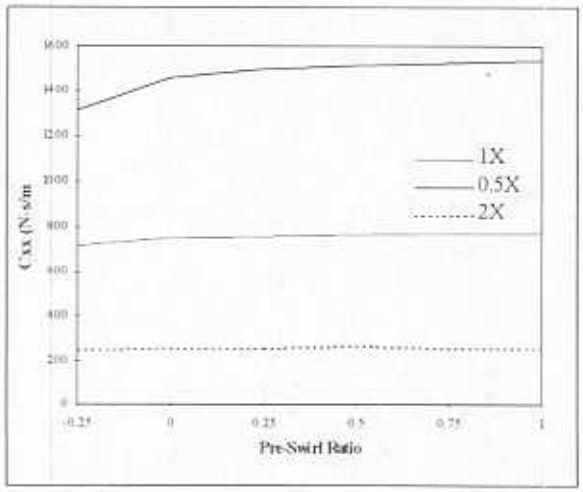


(c)

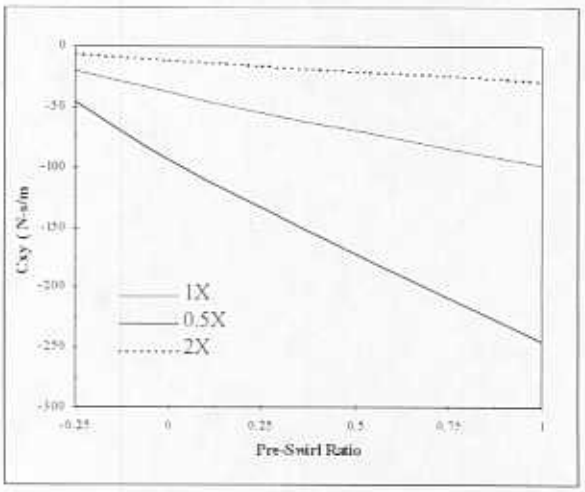


(d)

Fig. 13 Dynamic force coefficients of a two-bladed gas damper seal vs. inlet pre-swirl ratio
( inlet pressure=4.1347 bar, exit pressure=1.013 bar, Ω=9,000 rpm )

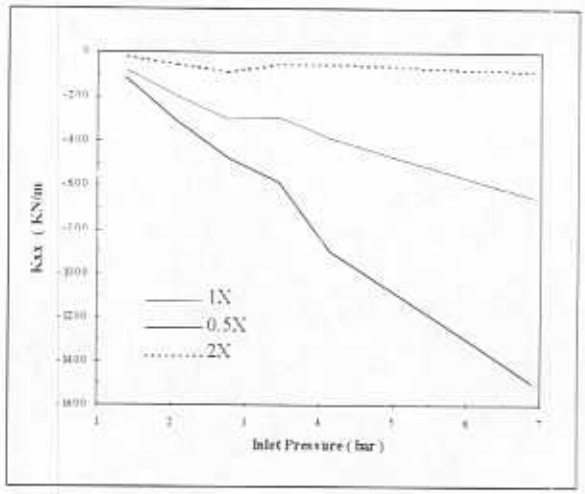


(a)

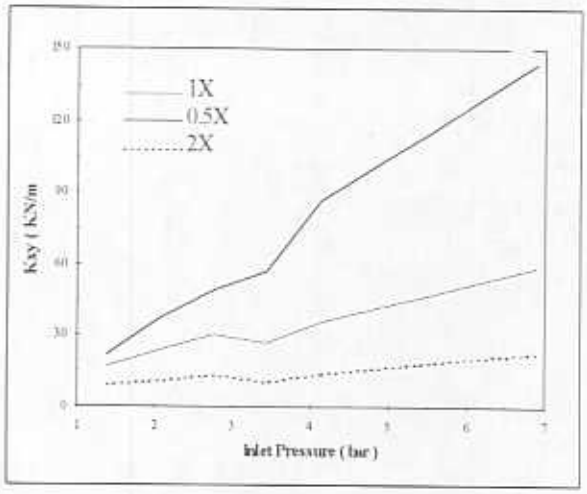


(b)

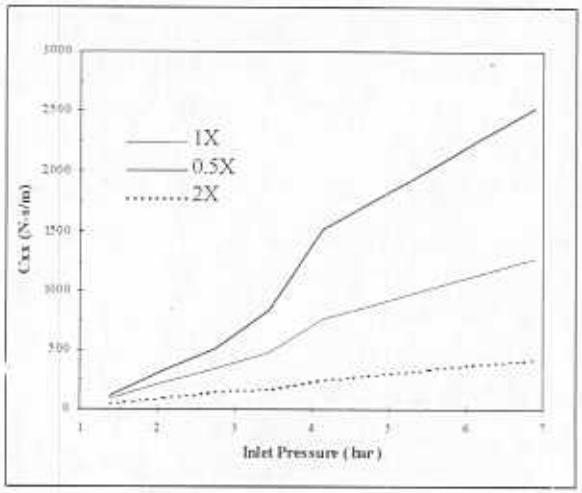


(c)

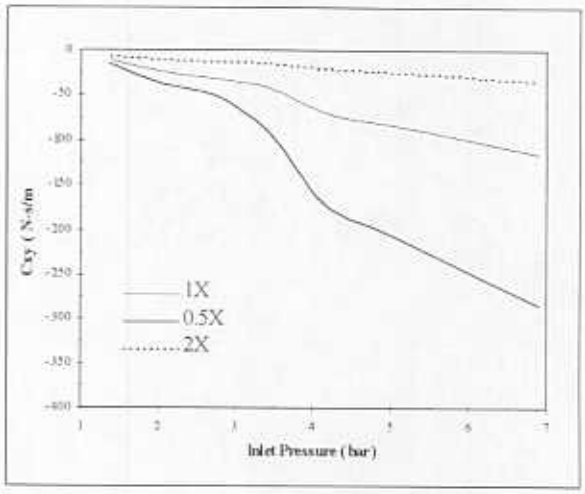


(d)

Fig. 14 Dynamic force coefficients of a two-bladed gas damper seal vs. inlet pressure ( exit pressure=1.013 bar, $\Omega$=9,000 rpm, pre-swirl ratio=0.5 )

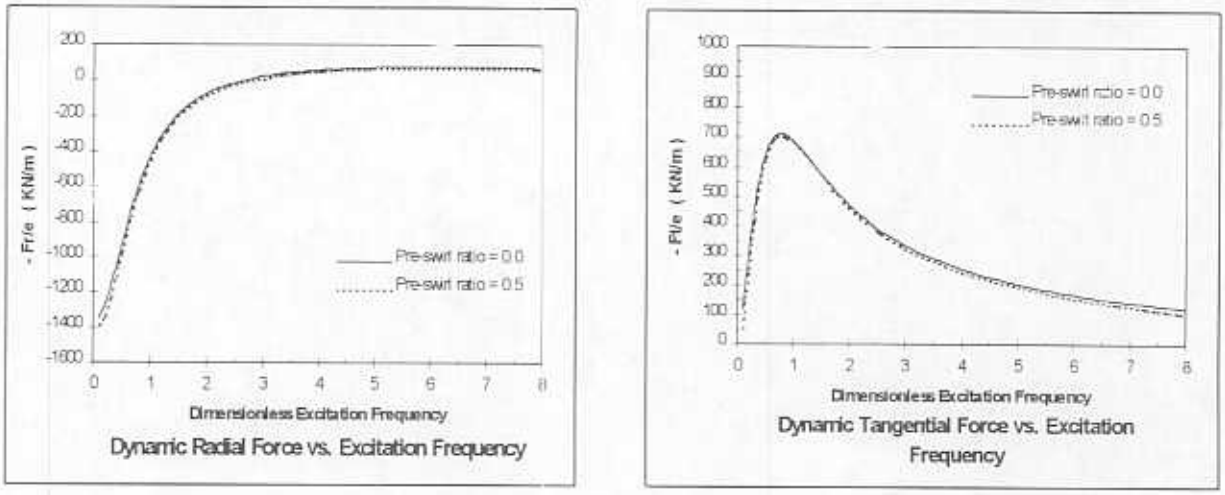


(a) (b)

**Fig. 15 Dynamic forces of a two-bladed gas damper seal vs. excitation frequency for two pre-swirl ratios**
**( Ω=9,000 rpm, inlet pressure=4.1347 bar, exit pressure=1.013 bar)**

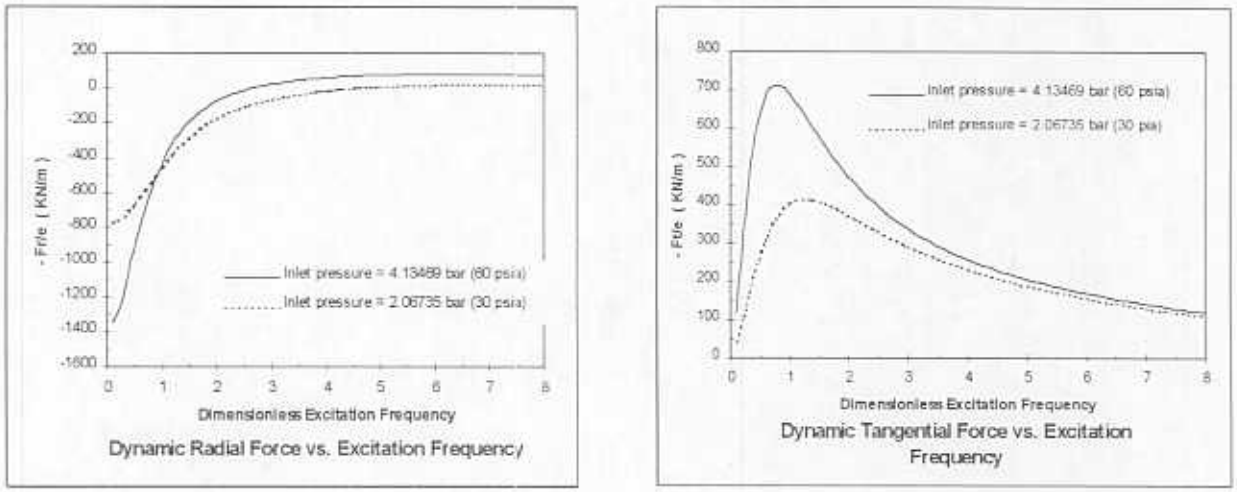


(a) (b)

**Fig. 16 Dynamic forces of a two-bladed gas damper seal vs. excitation frequency at two inlet pressures**
**( Ω=9,000 rpm, pre-swirl ratio=0.0, exit pressure=1.013 bar)**

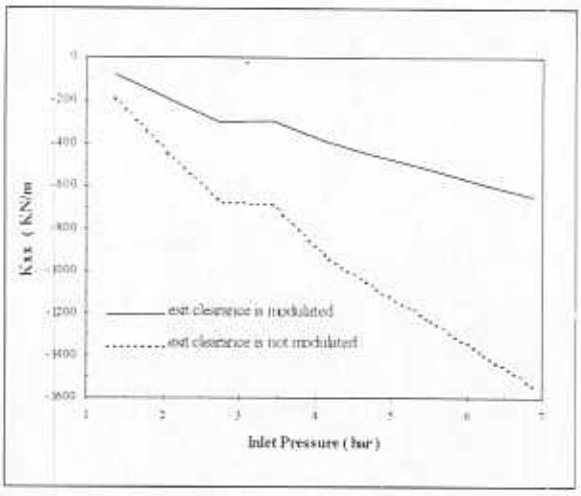


(a)

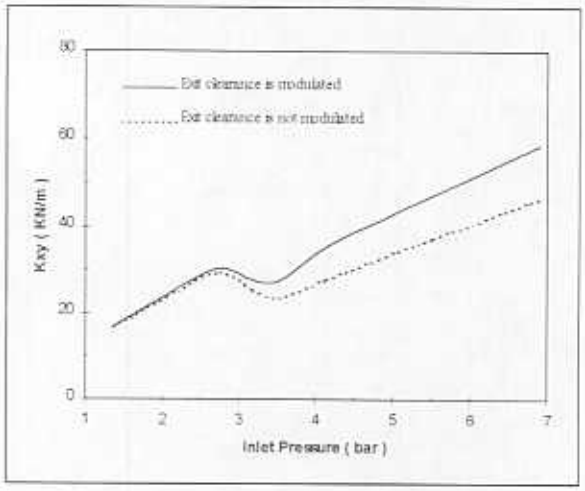


(b)

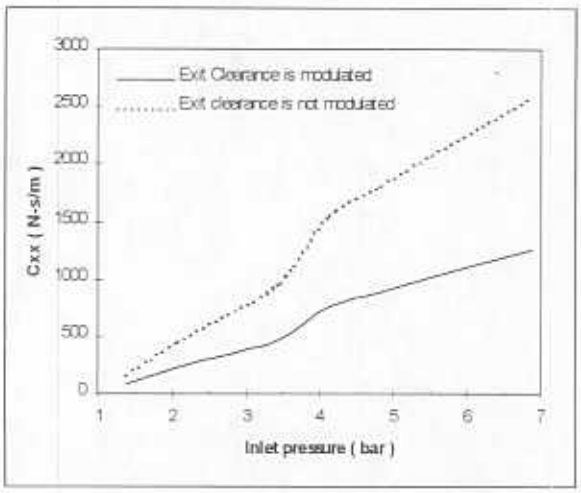


(c)

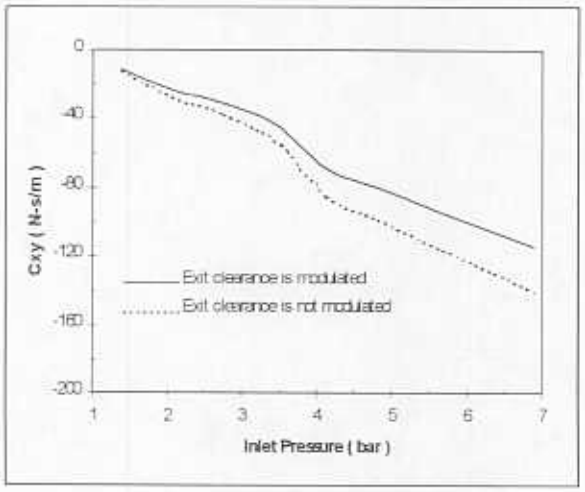


(d)

**Fig. 17 Dynamic force coefficients of a two-bladed gas damper seal with fixed and modulated exit clearances**
**( exit pressure=1.013 bar, pre-swirl ratio=0.5 )**
**( $\Omega$=9,000 rpm, $\omega$ = 150 Hz )**

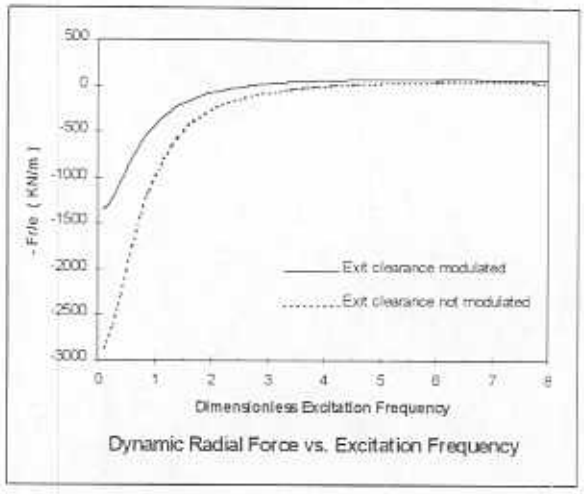


(a)

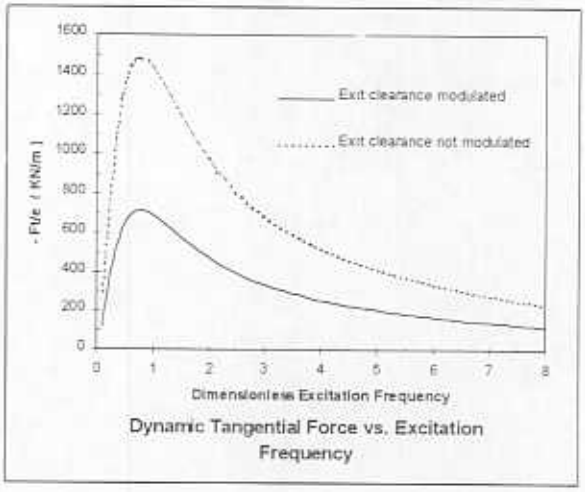


(b)

**Fig. 18 Radial and tangential dynamic forces of a two-bladed gas damper seal with fixed and modulated exit clearances**
**( inlet pressure=4.1347 bar, exit pressure=1.013 bar, pre-swirl ratio=0.5 )**
**( $\Omega$=9,000 rpm, $\omega$ = 150 Hz )**

## REFERENCES


Alford J. S., (1965), "Protecting Turbomachinery From Self-Excited Rotor Whirl," *ASME Journal of Engineering for Power*, October, pp. 333 - 344.

Brown, R. D., and Hart, J. A., (1986), "A novel form of Damper for Turbomachinery," Proceedings of The First European Sponsored Turbomachinery Symposium, October, pp. 55-63.

Childs, D. W., Elrod, D., and Hals, K., (1989), "Annular Honeycomb Seals: Test Results for leakage and Rotordynamic Coefficients; Comparisons to labyrinth and Smooth configurations," *ASME Journal of Tribology*, Vol. 111, pp. 293-301.

Childs, D. W., (1993), "Turbomachinery Rotordynamics: Phenomena, Modeling, & Analysis," John Wiley & Sons, Inc., pp. 300.

Childs, D. W. and Ramsey, C., (1990), "Seal- Rotordynamic coefficient test Results for a Model SSME ATD-HPFTP turbine Interstage Seal with and Without a Swirl Brake", Proceeding of a workshop on Rotordynamic Instability Problems in High-Performance Turbomachinery, Texas A&M University. pp. 172-184.

Childs, D. W., Elrod, D., and Ramsey, C., (1990a), "Annular Honeycomb Seals: Additional Test Results for leakage and Rotordynamic Coefficients," in IFToMM, Proceedings of the Third International Conference on Rotordynamics, Lyon, France, pp. 303-312.

Childs, D. W., Baskharone, E., and Ramsey, C., (1990b), "Test Results for Rotordynamic Coefficients of the SSME HPOTP Turbine Interstage Seal with Two Swirl Brakes," ASME paper # 90-Trib-40.

Childs, D. W., and Kleynhans, G., (1993), "Theory versus Experiment for Short (L/D=1/6) Honeycomb and Smooth Annular Pressure Seals," Proceedings of the 14th ASME Vibration and Noise Conference, September 19-22, Albuquerque, New Mexico. pp. 173-179

Childs, D. W., and Gansle, A. J., (1996), "Experimental Leakage and Rotordynamic Results for Helically Grooved Annular Gas Seals," *ASME Journal of Engineering for Gas Turbines and Power*, Vol. 118, pp. 389-393.

Hawkins, L, Childs, D. W., and Hale Keith, (1989), "Experimental Results for Labyrinth Gas Seals with Honeycomb Stator: Comparisons to smooth-Stator and Theoretical Predictions", ASME Journal of Tribilogy. Vol. 111, No. 1, pp.161-168.

Hirs, G., (1973), "A Bulk-Flow Theory for Turbulence in Lubrication Films," *ASME*

*Journal of Lubrication Technology*, Vol. 75, pp.137-146.

Kim, C. H., and Lee, Y. B., (1994), "Test Results for Rotordynamic Coefficients of Anti-Swirl Self-Injection Seals," ASME Journal of Tribology, Vol. 116, pp. 508-513.

Kleynhans, G., and Childs, D. W., (1996), "The Acoustic Influence of Cell Depth on the Rotordynamic Characteristics of Smooth-Rotor/Honeycomb-Stator Annular Gas Seals," Proceeding of a workshop on Rotordynamic Instability Problems in High-Performance Turbomachinery, Texas A&M University. pp. 129-140.

Laundar, B. E., and Leschziner, M., (1978), "Flow in Finite-Width, Thrust Bearings Including Inertial Effects, I - laminar Flow, II - Turbulent Flow," *ASME Journal of Lubrication Technology*, Vol. 100, pp. 330-345.

Li, J., (1995), "The Effect of A New Damper Seal on Rotordynamics," Master's Thesis, Texas A&M University.

Li, J., and Vance, J. M., (1995), "Effects of Clearance and Clearance Ratio on Two and Three Bladed TAMSEALs," TRC-Seal-4-95, Turbomachinery Laboratory.

Lund, J. W., (1987), "Review of The Concept of Dynamic Coefficients for Fluid Film Journal Bearings," *ASME Journal of Tribology*, Vol. 109, pp. 37-41.

Murphy, B. T., and Vance, J. M., (1980), "Labyrinth Seal Effects on Rotor Whirl Instability," Proceedings of the 2nd International Conference on Vibrations in Rotating Machinery (ImechE), #C306/80, pp. 369-373.

Patankar, S. V., (1980), Numerical Heat Transfer And Fluid Flow, Hemisphere Publishing Corporation, McGraw-Hill.

Richards, R. L., Vance, J. M., and Zeidan, F. Y., (1995), "Using A Damper Seal to Eliminate Subsynchronous Vibrations in Three Back-to-Back Compressors," Proceedings of 24th Turbomachinery Symposium, Houston, September, pp.59-71.

San Andres, L., (1990), "Turbulent Hybird Brearings With Fluid Inertia effects," *ASME Journal of Tribology*, Vol. 112, pp. 699-707.

San Andres, L., Yang, Z., and Childs, D.W., (1993), "Thermal Effects in Cryogenic Liquid Annular Seals - Part II: Numerical Solution and Results," *ASME Journal of Tribology*, Vol. 115, pp. 277-284.

Sundararajan, P., and Vance, J. M., 1995, "A Theoretical and Experimental

Investigation of a Gas-Operated Bearing Damper for Turbomachinery - Part II: Experimental Results and Comparison with Theory," *ASME Journal of Engineering for Gas Turbines and Power*, Vol. 117, pp. 750-756.

Van Doormaal, J. P., and Raithby, G. D., 1984, "Enahncements of the SIMPLE Method for Predicting Incompressible Fluid Flows," Numerical Heat Transfer, Vol. 7, pp. 147-163.

Vance, J. M., Cardon, B. P., San Andres, L. A., and Storace, A. F., (1993), "A Gas-Operated Bearing Damper for Turbomachinery," *ASME Journal of Engineering for Gas Turbines and Power*, Vol. 115, pp. 383-389.

Vance, J., and Handy, S. B., (1996), "Rotordynamic Instability From An Anti-Swirl Device," Proceeding of a workshop on Rotordynamic Instability Problems in High-Performance Turbomachinery, Texas A&M University, pp. 129-140.

Vance, J. M., and Li, J., (1996), "Test Results of A New Damper Seal for Vibration Reduction in Turbomachinery," *ASME Journal of Engineering for Gas Turbines and Power*, Vol. 118, pp. 843-846.

Vance, J. M., and Sundararajan, P., (1993), "Design And Applications Analysis of A New Damper Seal," TRC Meeting Report, Turbomachinery Laboratory.

Vance, J. M., and Schultz, R. R., 1993, "A New Damper Seal for Turbomachinery," in Vibration of Rotating System, *Proceedings of the 14th Vibration and Noise Conference*, Albuquerque, New Mexico, ASME DE-Vol. 60, pp. 139-148.

Vance, J. M., Zierer, J. J., and Conway, E. M., (1993), "Effect of Straight Through Labyrinth Seals on Rotordynamics," in Vibration of Rotating System, *Proceedings of the 14th Vibration and Noise Conference*, Albuquerque, New Mexico, ASME DE-Vol. 60, pp. 159-171.

Von Pragenau, G. L., (1982), "Damping Seals for Turbomachinery," NASA Technical Paper 1987.

Wright, D. V., (1983), "Labyrinth Seal Forces on A Whirling Rotor," Rotordynamic Instability, Proceedings of the ASME Applied Mech., Bioeng. and Fluids Engineering Conference, Houston, Texas, pp.19 - 31.

Yang, Z., San Andres, L., and Childs, D. W., (1993), "Dynamic Force Performance of Annular Gas Seals at Off-Center Conditions," STLE paper, #93-AM-4D-1.

Yu, Z., and Childs, D. W., (1997), "A Comparison of Experimental Rotordynamic Coefficients and Leakage Characteristics Between Hole-Pattern Gas Damper Seals and A

Honeycomb Seal," accepted for ASME Turb Expo'97 Conference, Orlando, FL, June, 1997.

Zeidan, F. Y., Perez, R. X, and Stephenson, E. M., (1993), "The use of Honeycomb Seals in Stabilizing Two Centrifugal Compressors," Proceedings of the 22nd Turbomachinery Symposium, Dallas, September, pp.3-15.

**Additional References**

Scharrer, J., (1988), "Theory Versus Experiment for the Rotordynamic Coefficients of Labyrinth Gas Seals: Part I - A Two Control Volume Model," *ASME Journal of Vibration, Acoustics, Stress, and Reliability in Design*, Vol. 110, pp. 270-280.